We are IntechOpen,
the world's leading publisher of
Open Access books
Built by scientists, for scientists

6,900
Open access books available

185,000
International authors and editors

200M
Downloads

154
Countries delivered to

Our authors are among the

TOP 1%
most cited scientists

12.2%
Contributors from top 500 universities

CLARIVATE ANALYTICS
BOOK CITATION INDEX
INDEXED

WEB OF SCIENCE™

Selection of our books indexed in the Book Citation Index
in Web of Science™ Core Collection (BKCI)

Interested in publishing with us?
Contact book.department@intechopen.com

Numbers displayed above are based on latest data collected.
For more information visit www.intechopen.com

Numerical Simulation of Elastic-Plastic Non-Conforming Contact

Sergiu Spinu, Gheorghe Frunza and Emanuel Diaconescu
Department of Applied Mechanics, University "Stefan cel Mare" of Suceava
Romania

1. Introduction

A fast algorithm for elastic-plastic non-conforming contact simulation is presented in this work. While the elastic response of a material subjected to load application is reversible, plasticity theory describes the irreversible behavior of the material in reaction to loading beyond the limit of elastic domain. Therefore, elastic-plastic response of contacting bodies to loading beyond yield strength is needed to assess the load-carrying capacity of the mechanical contact.

The modern approach in simulating elastic-plastic contact is based on the algorithm originally proposed by Mayeur, (Mayeur, 1996), employing Betti's reciprocal theorem. Although Mayeur developed a model for the three-dimensional problem, numerical implementation was restricted to two-dimensional case, due to lack of formulas for the influence coefficients.

Problem generalization is due to Jacq, (Jacq, 2001), and to Jacq et al. (Jacq et al., 2002), who advanced a complete semi-analytical formulation for the three-dimensional elastic-plastic contact. The algorithm was later refined by these authors, (Wang & Keer, 2005), who improved the convergence of residual and elastic loops. The main idea of their Fast Convergence Method (FCM) is to use the convergence values for the current loop as initial guess values for the next loop. This approach reduces the number of iterations if the loading increments are small.

Nélias, Boucly, and Brunet, (Nélias et al., 2006), further improved the convergence of the residual loop. They assessed plastic strain increment with the aid of a universal algorithm for integration of elastoplasticity constitutive equations, originally proposed by Fotiu and Nemat-Nasser, (Fotiu & Nemat-Nasser, 1996), as opposed to existing formulation, based on Prandtl-Reuss equations, (Jacq, 2001). As stated in (Nélias et al., 2006), this results in a decrease of one order of magnitude in the CPU time.

Influence of a tangential loading in elastic-plastic contact was investigated by Antaluca, (Antaluca, 2005). Kinematic hardening was added by Chen, Wang, Wang, Keer, and Cao, (Chen et al.,2008), who advanced a three-dimensional numerical model for simulating the repeated rolling or sliding contact of a rigid sphere over an elastic-plastic half-space.

The efficiency of existing elastic-plastic contact solvers, (Jacq et al., 2002; Wang & Keer, 2005) is impaired by two shortcomings. Firstly, the algorithms are based on several levels of iteration, with the innermost level having a slow convergence. Secondly, the effect of a three-dimensional distribution in a three-dimensional domain, namely residual stresses related to plastic strains, is computed using two-dimensional spectral algorithms.

A numerical approach to simulate the elastic-plastic contact, based on Betti's reciprocal theorem, is overviewed in this work. Computation of residual stresses due to plastic strains is accelerated by implementing three-dimensional spectral methods, in a hybrid convolution-correlation algorithm. Pressure-free surface condition in Chiu's inclusion problem decomposition is imposed with the aid of Boussinesq fundamental solutions and superposition principle. The newly proposed algorithm appears well adapted to numerical simulation of elastic-plastic contacts. Fotiu and Nemat-Nasser's universal algorithm is employed to derive plastic strain increment. The convergence of the residual part is therefore improved dramatically, and computationally intensive residual stress assessment is moved to an upper iterative level, allowing for finer resolutions in problem digitization.

2. Formulation of continuous elastic-plastic contact problem

Since the works of Mayeur, (Mayeur, 1996), and Jacq, (Jacq, 2001), Betti's reciprocal theorem is used in elastic-plastic contact modeling to assess surface normal displacement and stress state in an elastic half-space in the presence of plastic strains. The basis of Betti's theorem is the equality between the work done by the virtual force through the displacements produced by the real force and the work done by the real force through the displacements produced by the virtual force.

According to this formulation, if two independent loads are applied to an elastic body of volume Ω and of boundary Γ, generating two independent states (u, ε, σ) and $(u^*, \varepsilon^*, \sigma^*)$ with vanishing body forces, and the latter corresponds to a unit load applied along the direction of $\vec{x}_3$, in a point A of the boundary (a unit impulse):

$$p_3^*(M) = \begin{cases} 0, & M \neq A; \\ (dx_1 dx_2)^{-1}, & M = A, \end{cases} \tag{1}$$

the following equation holds:

$$u_3(A) = \int_{\Gamma_C} u_{33}^*(M, p_3^*(A)) p_3(M) d\Gamma + 2\mu \int_{\Omega_p} \varepsilon_{ij}^p(M) \varepsilon_{3ij}^*(M, p_3^*(A)) d\Omega. \tag{2}$$

Here, Γ_C is the boundary subdomain with normal tractions p_3 defined, and Ω_p the volume subdomain with existing plastic strains ε^p, both corresponding to state (u, ε, σ), μ Lamé's constant and M the integration point. This point is located within Γ_C in the first term of Eq. (2) and within Ω_p in the second. Consequently, $u_{33}^*(M, p_3^*(A))$ is the displacement in the direction of $\vec{x}_3$, and $\varepsilon_{3ij}^*(M, p_3^*(A))$ is the strain tensor induced at point M by the loading described by Eq. (1). By varying the position of A on Γ and by applying superposition principle with respect to integration point M, normal displacement in every point of the boundary can be assessed.

The second term in Eq. (2), which is expressed as a volume integral, represents the residual part of displacement, namely the deflection that would persist after unloading elastically the considered body. Knowledge of normal residual displacement allows solving the elastic-plastic contact problem as a purely elastic problem with a modified initial contact geometry. A level of iteration, corresponding to solution of elastic contact, is therefore required for the mutual adjustment between contact pressure and surface normal displacement.

Betti's reciprocal theorem is also applied to assess stress state in the half-space, in the presence of plastic strains. As shown in the following section, knowledge of stress state and of hardening state of the elastic-plastic material allows for computation of plastic strain increment, when a new loading increment is applied leading to further yielding. Again, two independent loads are considered, leading to two independent states (u, ε, σ) and $(u^{**}, \varepsilon^{**}, \sigma^{**})$, the latter corresponding to a unit load applied along the direction of $\vec{x}_k$, in a point B inside the half-space:

$$p_k^*(M) = \begin{cases} 0, & M \neq B; \\ (dx_1 dx_2 dx_3)^{-1}, & M = B, \end{cases} \tag{3}$$

The following equation yields from the general form of Betti's reciprocal theorem:

$$u_k(B) = 2\mu \int_{\Omega_p} \varepsilon_{ij}^p(M) \varepsilon_{kij}^{**}(M, B) d\Omega + \int_{\Gamma_C} u_{3k}^{**}(M, B) p_3(M) d\Gamma. \tag{4}$$

Here, $u_{3k}^{**}(M, B)$ and $\varepsilon_{kij}^{**}(M, B)$ are the displacement along direction of $\vec{x}_3$ and the ij strain tensor component respectively, induced at point M in the half-space by the unit load applied at point B along the direction of $\vec{x}_k$. By varying the position of B in Ω and by applying superposition principle with respect to integration point M, displacements in every point of the body can be assessed.

Eq. (4) suggests that stresses have an "elastic" part, σ^{pr}, related to contact pressure p_3, which is expressed as a surface integral over Γ_C, and a residual part, σ^r, expressed as a volume integral over plastic region Ω_p. The term "elastic" in the previous statement can be misleading, as all stresses are elastic, but σ^{pr} denotes the part of stresses that would vanish if an elastic unloading would occur. This stresses are related to contact pressure, as opposed to residual stresses σ^r, which are linked to the plastic region Ω_p, and would persist after elastic unloading. If $M_{ijk\ell}$ is the stiffness tensor from Hooke's law, the following equations hold:

$$\sigma_{ij}^{pr} = M_{ijk\ell}\left(\frac{1}{2}(u_{k,\ell}^{pr} + u_{\ell,k}^{pr})\right), \quad u_k^{pr}(B) = \int_{\Gamma_C} u_{k3}^{**}(M, B) p_3(M) d\Gamma, \tag{5}$$

$$\sigma_{ij}^{r} = M_{ijk\ell}\left(\frac{1}{2}(u_{k,\ell}^{r} + u_{\ell,k}^{r}) - \varepsilon_{k\ell}^p\right), \quad u_k^{r}(B) = 2\mu \int_{\Omega_p} \varepsilon_{ij}^p(M) \varepsilon_{kij}^{**}(M, B) d\Omega. \tag{6}$$

A single comma in the subscript denotes the derivative with respect to the corresponding direction: $u_{i,j} = \partial u_i / \partial x_j$.

Resulting equations (2) and (4) suggest elastic-plastic contact problem split in an "elastic" and a residual part. As shown in the following sections, the elastic part comprises the static force equilibrium, interference equation, and complementarity conditions, while the residual part expresses the plastic strain increment and plastic zone contribution to surface normal displacement and to stress state in the elastic-plastic body.

However, the two subproblems cannot be solved independently, as residual displacement, computed in the residual part, enters interference equation in the elastic part, while contact

stress, assessed in the elastic subproblem, is needed to find the plastic strain increment in the residual part.

Analytical resolution of resulting model is available for neither the elastic, nor the residual part, as integration domains, namely boundary region with tractions and plastic strain volume respectively, not known a priori, are arbitrarily shaped. Therefore, numerical approach is preferred.

The principle of numerical approach consists in considering continuous distributions as piece-wise constant on the cells of a three-dimensional grid imposed in a volume enveloping integration domains. Continuous integration in the analytical model of the elastic-plastic contact model is replaced by multi-summation of elementary cells individual contributions. As these multi-summation operations are in fact convolution and/or correlation products, spectral methods are applied to speed up the computation.

3. Numerical solution of the elastic part

The numerical model of the elastic part is obtained from that corresponding to a normal elastic contact problem completed with the residual term, which is superimposed into the interference equation.

Numerical resolution of elastic contact problem relies on considering continuous distributions as piecewise constant on the elements of a rectangular mesh imposed in the common plane of contact and including the contact area. This approach allows transforming the integral contact equation, for which analytical solutions exists only in a few cases, in a linear system of equations, having nodal pressure as unknowns.

Kalker and van Randen, (Kalker & van Randen, 1972), reformulated the elastic contact problem as a problem of minimization, where the unknown contact area and pressure distribution are those who minimize the total complementary energy, under the restrictions that pressure is positive on the contact area and there is no interpenetration. This formulation finally reduces to solving a set of equations and inequalities which have to be satisfied simultaneously:

$$h(i,j) = hi(i,j) + u^{pr}(i,j) - \omega , (i,j) \in D \tag{7}$$

$$h(i,j) = 0, p(i,j) > 0 , (i,j) \in A \tag{8}$$

$$h(i,j) > 0, p(i,j) = 0 , (i,j) \in D - A \tag{9}$$

$$\Delta \sum_{(i,j) \in A} p(i,j) = W \tag{10}$$

with: h – the gap between the deformed contact surfaces; hi – the initial gap (without loading); u^{pr} – the composite displacements of the contact surfaces, due to contact pressure; ω - rigid-body approach; W – the load transmitted through contact; A - digitized contact area; D - digitized computational domain. A set of two integers (i,j) is used in the numerical model instead of continuous coordinates x_i to denote patch position in the grid.

This numerical formulation cannot predict singularities in the computed fields, as it employs values averaged over the elementary patches, but allows for the use of influence coefficients based methods. The most efficient approach in solving the system (7)-(10)

employs a modified conjugate gradient method (CGM), originally proposed by Polonsky and Keer, (Polonsky & Keer, 1999). This algorithm has two main advantages over other minimization methods. Firstly, convergence is assured, as there is proof of convergence for the CGM, and the rate of convergence is superlinear. Theory states, (Shewchuk, 1994), that CGM should converge in a number of iterations equal to the number of non-nil unknowns, namely the numbers of cells in contact. In practice, a much faster convergence was observed for smooth contact geometries. Secondly, the algorithm allows for imposing additional restrictions in the course of CG iterations. This means contact area is iterated during pressure correction, based on non-adhesion, Eq. (8), and non-penetration principles, Eq. (9). The force balance condition, Eq. (10), is also imposed to correct the pressure distribution. This eliminates the need for additional nested loops, which were present in most contact solvers prior to this approach.

Convolution product is used to derive the answer of a linear elastic system subjected to an input, when the unit impulse response, also referred to as the Green function, is known. For contact problems, the response of an elastic isotropic half-space to a unit concentrated force applied on the boundary is known from the Boussinesq and/or Cerruti fundamental solutions. The product of this solution (or Green function) with a shape function, as defined in (Liu et al., 2000), yields the influence coefficient (IC), which expresses contribution of an element of the grid into another. Superposition principle is then applied, implying summation of individual contributions over all grid elements. This multi-summation process, which is in fact a convolution product, is very time-consuming, being of order $O(N^2)$ for a grid with N elementary patches.

In order to circumvent this limitation, the solution currently applied is to compute the convolution in the frequency domain, according to convolution theorem, thus reducing the computational effort to $O(N \log N)$. An important issue when using discrete cyclic convolution to assess continuous linear convolution is the periodization of the problem, which induce the so called periodicity error, (Liu et al., 2000). If the Green function is known in the time-space domain, the Discrete Convolution Fast Fourier Transform (DCFFT) technique proposed by these authors, (Liu et al., 2000), eliminates completely the periodicity error, as discrete cyclic convolution approaches the linear continuous convolution the way quadrature estimates continuous integral.

The implemented algorithm for solving numerically the elastic contact problem, described in detail in (Spinu et al., 2007), can be summarized in the following steps:

1. Acquire the input: contact geometry, elastic properties of the contacting materials, normal load transmitted through contact.
2. Establish the computational domain, D. For non-conforming contact problems, Hertz contact area usually makes a good guess value. If during pressure iterations, current contact area is not kept inside computational domain, namely $A^{(k)} \not\subset D$, the algorithm should be restarted with a new D.
3. Establish grid parameters, based on available computational resources.
4. Choose the guess value for pressure, $\mathbf{p}^{(0)}$ and the imposed precision *eps* for the conjugate gradient iteration. According to (Polonsky & Keer, 1999), the latter should be correlated with the number of grids.
5. Start the conjugate gradient loop. Compute surface normal displacement field as a convolution between influence coefficients matrix $\mathbf{K}$ and current pressure $\mathbf{p}^{(k)}$, using DCFFT for computational efficiency: $\mathbf{u}^{(k)} = \mathbf{K} \otimes \mathbf{p}^{(k)}$, where symbol "$\otimes$" is used to denote two-dimensional discrete cyclic convolution.

6. Compute the gap distribution, corresponding to residual in CG formulation, using Eq. (7) with a vanishing rigid body approach ω: $h^{(k)}(i,j) = hi(i,j) + u^{(k)}(i,j)$, $(i,j) \in D$. In order to compensate for the disregarding of ω (which is unknown), $\mathbf{h}^{(k)}$ is normalised by its mean value on the current contact area $A^{(k)}$.

7. Compute the descent direction $d^{(k)}(i,j)$ in the CG algorithm.

8. Compute the length of the step $\alpha^{(k)}$ to be made along minimization direction: $\mathbf{t}^{(k)} = \mathbf{K} \otimes \mathbf{d}^{(k)}$, $\alpha = \mathbf{h}^{(k)}\mathbf{d}^{(k)}\left(\mathbf{t}^{(k)}\mathbf{d}^{(k)}\right)^{-1}$. For consistence with gap correction in step 6, $\mathbf{t}^{(k)}$ is also normalized by its mean value.

9. Adjust nodal pressures: $p^{(k+1)}(i,j) = p^{(k)}(i,j) + \alpha d^{(k)}(i,j)$.

10. Impose complementarity conditions. Cells with negative pressure are excluded from current contact area $A^{(k)}$, and the corresponding nodal pressures are set to zero. Cells with negative gap re-enter $A^{(k)}$, and the corresponding pressures are adjusted according to step 9.

11. Verify convergence criterion: $\left|\mathbf{p}^{(k+1)} - \mathbf{p}^{(k)}\right| \leq eps$.

The model was enhanced to allow for eccentric loading of conforming contacts by these authors, (Spinu & Diaconescu, 2008), who imposed an additional Newton-Raphson iterative level to allow for rotation of common plane of contact. Later on, Spinu (Spinu, 2008) further improved the algorithm, by suppressing the outer iterative level and by imposing a correction of tilting angles of contact common plane during CG iterations.

4. Numerical solution of the residual part

4.1 Plastic zone contribution to surface displacement

The residual part is also reformulated numerically, by imposing digitized plastic strain distribution and finite load increments. As the region of plastic strains Ω_p can be arbitrarily shaped, the integrals in Eq. (2) can only be computed numerically. The numerical formulation is based on dividing Ω_p in a set of N cuboids of elementary volume Ω_c, having uniform plastic strains in each elementary cuboid. Consequently, the continuous distribution of $\boldsymbol{\varepsilon}^p$ in Ω_p is assumed as piece-wise constant and Ω_p is substituted by a set of elementary cuboids Ω_{pn}. With this formulation, the residual displacement can be expressed as the sum of contributions of all elementary cuboids in Ω_{pn}:

$$u_3^r(A) = 2\mu \sum_{k=1}^{N} \varepsilon_{ij}^p(k) \int_{\Omega_c} \varepsilon_{3ij}^*(k,A) , \tag{11}$$

or, by indexing the cuboids with a set of three integers, and by denoting the cuboid sides with Δ_1, Δ_2 and Δ_3:

$$u_3^r(i,j,0) = 2\mu \sum_{(\ell,m,n) \in \Omega_{pn}} \left\{ \varepsilon_{\zeta\xi}^p(\ell,m,n) \times \right.$$
$$\left. \int_{x_3(n)-\Delta_3/2}^{x_3(n)+\Delta_3/2} \int_{x_2(m)-\Delta_2/2}^{x_2(m)+\Delta_2/2} \int_{x_1(\ell)-\Delta_1/2}^{x_1(\ell)+\Delta_1/2} \varepsilon_{3\zeta\xi}^*\left(\ell - x_1(i), m - x_2(j), n\right) dx_1 dx_2 dx_3 \right\}. \tag{12}$$

The tensor ε_3^*, representing strains due to a unit concentrated force applied on surface boundary, is known from Boussinesq fundamental solutions, (Boussinesq, 1969), which represent, in terms of spectral methods, the corresponding Green functions. In order to compute the influence coefficients, functions d_{ii} are defined as primitives of functions $2\mu\varepsilon_{3ii}^* = \mu(u_{3i,i}^* + u_{3i,i}^*)$ with respect to directions of $\vec{x}_1, \vec{x}_2$ and of $\vec{x}_3$, and functions d_{ij}, $i < j$, as primitives of $2\mu\left(\varepsilon_{3ij}^* + \varepsilon_{3ji}^*\right) = 2\mu(u_{3i,j}^* + u_{3j,i}^*)$ with respect to the same directions. The influence coefficients can then be computed according to the formulas given in (Spinu, 2009).

Eq. (12) written with respect to indices of elementary cells takes the following form:

$$u_3^r(i,j,0) = \sum_{(\ell,m,n)\in\Omega_{pn}} \varepsilon_{\zeta\xi}^p(\ell,m,n)D_{\zeta\xi}\left(\ell-i,m-j,n\right), \tag{13}$$

with summation over $\zeta,\xi = 1,2,3$, $\zeta \leq \xi$. If expression $D_{\zeta\xi}\left(i-\ell,j-m,n\right)$ is used in relation (13) instead of $D_{\zeta\xi}\left(\ell-i,m-j,n\right)$, namely the point of integration and the point of observation are interchanged, Eq. (13) takes the following form:

$$u_3^r(i,j,0) = \sum_{(\ell,m,n)\in\Omega_{pn}} D_{\zeta\xi}\left(i-\ell,j-m,n\right)\varepsilon_{\zeta\xi}^p(\ell,m,n), \tag{14}$$

which represents a discrete cyclic convolution with respect to directions of $\vec{x}_1$ and of $\vec{x}_2$. Efficient computation for this product is available through DCFFT, (Liu et al., 2000).

4.2 Plastic zone contribution to stress state

The problem of residual stresses due to plastic zone in elastic-plastic contact can be treated in the more general frame of the so called "inclusion problem". Eigenstrains such as plastic strains, misfits strains, thermal expansion or phase transformation, generate a linear elastic stress field in an isotropic half-space. Usually, assessment of this field, also referred to as the inclusion problem, is performed using a problem decomposition method originally suggested by Chiu, (Chiu, 1978). Although inclusion problem has received a great deal of attention in the last four decades, (Mura, 1988), closed form solutions exist only in a few cases of simple, regular shapes, such as spherical or cuboidal eigenstrains. In elastic-plastic contact modeling, these limiting assumptions are not met, thus imposing the use of numerical approach.

The problem of residual stresses arising in elastic-plastic contact was solved by Mayeur, (Mayeur, 1995), for the two-dimensional rough contact. The three-dimensional case was solved by Jacq, (Jacq, 2001), using Chiu's problem decomposition, (Chiu, 1978). These authors, (Jacq et al., 2002), used two-dimensional fast Fourier transform algorithms to efficiently compute the arising convolution products. Wang and Keer, (Wang & Keer, 2005), used a similar approach in studying residual stresses arising in elastic-plastic contact with hardening behavior. They stated that two-dimensional DCFFT should be applied in residual stress computation.

An alternative to Chiu's problem decomposition was advanced by Liu and Wang, (Liu & Wang, 2005), based on Mindlin and Cheng's results, (Mindlin & Cheng, 1950), involving derivatives of four key integrals. They also advanced an efficient algorithm to compute

correlation products using convolution theorem, called Discrete Correlation Fast Fourier Transform (DCRFFT).

Jin, Keer, and Wang, (Jin et al., 2008), suggested that, in order to achieve a better computational efficiency, convolution and correlation should be used together, in a hybrid algorithm. They presented some comparative results obtained using both two-dimensional and three-dimensional spectral algorithms, proving that the latter reduces dramatically the CPU time and memory requirements, allowing for finer grids.

The problem of elastic fields due to arbitrarily shaped inclusions in an elastic half-space was also treated by these authors, (Zhou et al., 2009). Although Chiu's problem decomposition is employed, influence coefficients for imposing the pressure-free surface condition are not derived explicitly, as stresses due to spurious pressure on the boundary are not expressed as functions of existing eigenstrains.

Mura, (Mura, 1968), stated that, in the presence of initial strains, a finite body with a traction-free surface can be treated as an infinitely extended body, if equal and opposite normal and shear stresses are applied on the boundary, compensating for the ones corresponding to the full space solution. Consequently, the method suggested by Chiu, (Chiu, 1978) consists in applying superposition principle to elastic states (b), (c), and (d) in Fig. 1, whose summation yields the elastic state of the original problem (a).

Eigenstrains in state (b) are identical to those of the original problem (a), while in state (c), the cuboid is the mirror image of the original one with respect to half-space boundary. Eigenstrains in state (c) are chosen such as shear tractions induced by states (b) and (c) cancel each-other on the half-space boundary:

$$\boldsymbol{\varepsilon}^{pm} = \boldsymbol{\varepsilon}^p \text{ , except for } \varepsilon_{13}^{pm} = -\varepsilon_{13}^p \text{ , and } \varepsilon_{23}^{pm} = -\varepsilon_{23}^p \text{ ,} \tag{15}$$

leading to a spurious normal traction (or pressure) depicted by state (d). Consequently, in order to simulate the traction-free boundary condition, solution of state (d) should be extracted from summation of solutions corresponding to states (b) and (c).

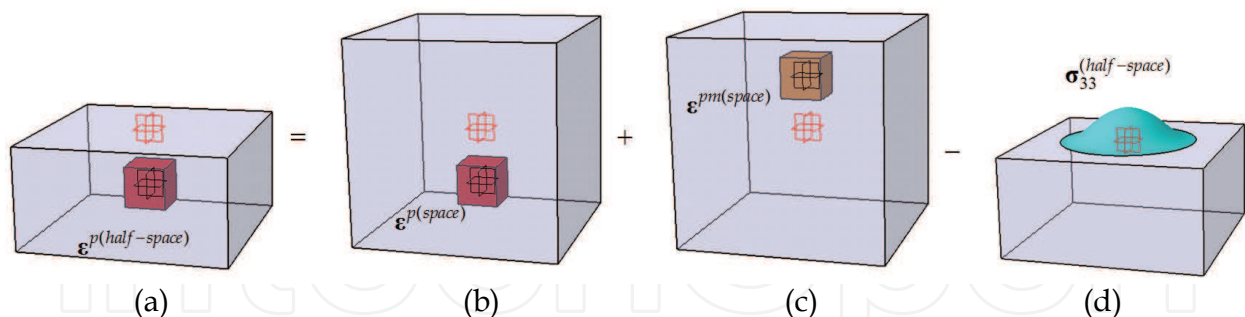(a)   (b)   (c)   (d)

Fig. 1. Inclusion problem decomposition: a. cuboidal inclusion in elastic half-space; b. cuboidal inclusion in infinite elastic space; c. an image counterpart in infinite space; d. a half-space with a pressure distribution

A uniformly-spaced rectangular grid is established in a cuboidal domain including the arbitrarily shaped plastic zone. According to superposition principle, problem solution is obtained by superimposing the solution of each cuboidal inclusion. If the grid is uniformly spaced, the number of different influence coefficients to be computed is reduced to the number of different distances between cell control points. This allows reformulation of multi-summation operation as a discrete convolution, which can be evaluated efficiently in the frequency domain, according to convolution and/or correlation theorems.

Plastic strains are assumed constant in every elementary cell, but otherwise can vary along computational domain. The solution for a cuboidal inclusion of constant eigenstrains in an infinite space, namely the IC, is needed.

The first closed form solution for the ICs required to assess states (b) and (c) in Fig. 1 was advanced by Chiu, (Chiu, 1977). A Cartesian coordinate system (x'_1, x'_2, x'_3) is attached to the centre of the cuboid. In the presence of plastic strains ε^p_{ij}, displacements u_i are related to strains by the strain-displacement equations:

$$\varepsilon^e_{ij} + \varepsilon^p_{ij} = \frac{1}{2}\left(u_{i,j} + u_{j,i}\right), \tag{16}$$

where $\boldsymbol{\varepsilon}^e$ is the elastic component of strains. By substituting ε^e_{ij} into the constitutive equation (Hooke's law), one can find the stresses induced by the eigenstrains ε^p_{ij}. The gradients of displacements needed in Eq. (16) were obtained by Chiu, (Chiu, 1977), using the Galerkin vector:

$$2\mu u_{i,q}(x'_1, x'_2, x'_3) = \frac{1}{8\pi^3}\sum_{m=1}^{8}(-1)^m\left[\begin{array}{l}\dfrac{1-2\nu}{1-\nu}\lambda\varepsilon^p_{kk}D_{,iqnn}(\mathbf{c}_m) + 4\mu\varepsilon^p_{ij}D_{,jqnn}(\mathbf{c}_m) - \\[2mm] -\dfrac{2\mu}{1-\nu}\varepsilon^p_{nj}D_{,iqnj}(\mathbf{c}_m)\end{array}\right], \tag{17}$$

where μ and λ are Lamé's constants, $\mathbf{c}_m$, $m = \overline{1,8}$ are the eight vectors linking the corners of the cuboid to the observation point, and $D(\mathbf{c}_m)$ is a function whose fourth derivates with respect to coordinates x'_j are obtained by circular permutation in one of four categories, $D_{,1111}$, $D_{,1112}$, $D_{,1122}$ and $D_{,1123}$, given in (Chiu, 1977). Einstein summation convention is employed in Eq. (17).

Summation of elastic fields induced by $\boldsymbol{\varepsilon}^p$ and $\boldsymbol{\varepsilon}^{pm}$ in a coordinate system with the origin on the half-space boundary yields the following equation:

$$\sigma^{(space)}_{ij}(x_1, x_2, x_3) = A_{ijk\ell}(x_1 - x'_1, x_2 - x'_2, x_3 - x'_3)\varepsilon^p_{k\ell}(x'_1, x'_2, x'_3) + \\ A_{ijk\ell}(x_1 - x'_1, x_2 - x'_2, x_3 + x'_3)\varepsilon^{pm}_{k\ell}(x'_1, x'_2, -x'_3). \tag{18}$$

where (x_1, x_2, x_3) is the observation point and (x'_1, x'_2, x'_3) the source point (the control point of the elementary cuboid having uniform plastic strains).

As all distributions are assumed piece-wise constant, it is convenient to index the collection of cuboids by a sequence of three integers ranging from 1 to N_1, N_2 and N_3 respectively, with $N = N_1 N_2 N_3$, and to express all distributions as functions of these integers instead of coordinates.

After superimposing the individual contributions of all cuboids, Eq. (18) becomes:

$$\sigma^{r(space)}_{\xi\zeta}(i, j, k) = \sum_{\ell=1}^{N_1}\sum_{m=1}^{N_2}\sum_{n=1}^{N_3}A_{\xi\zeta\varsigma\gamma}(i-\ell, j-m, k-n)\varepsilon^p_{\varsigma\gamma}(\ell, m, n) + \\ \sum_{\ell=1}^{N_1}\sum_{m=1}^{N_2}\sum_{n=1}^{N_3}A_{\xi\zeta\varsigma\gamma}(i-\ell, j-m, k+n)\varepsilon^p_{\varsigma\gamma}(\ell, m, n), \tag{19}$$

which expresses the stress field induced in infinite space at cell (i, j, k) by all cuboids of uniform eigenstrains (ℓ, m, n) and by their mirror images.

Based on this development, the spurious normal traction induced on the half-space boundary, $\sigma_{33}^{(half-space)}$, needed to solve the state (d) in Fig. 1, can be expressed:

$$\sigma_{33}^{(half-space)}(i, j) = \sigma_{33}^{r(space)}(i, j, 0) = \sum_{\ell=1}^{N_1} \sum_{m=1}^{N_2} \sum_{n=1}^{N_3} A_{33\varsigma\gamma}(i-\ell, j-m, -n)\varepsilon_{\varsigma\gamma}^p(\ell, m, n) +$$
$$\sum_{\ell=1}^{N_1} \sum_{m=1}^{N_2} \sum_{n=1}^{N_3} A_{33\varsigma\gamma}(i-\ell, j-m, n)\varepsilon_{\varsigma\gamma}^p(\ell, m, n), \qquad (20)$$

The stress induced in the half-space by this fictitious traction can then be computed:

$$\sigma_{\zeta\xi}(i, j, m) = \sum_{k=1}^{N_1} \sum_{\ell=1}^{N_2} Q_{\zeta\xi}(i-k, j-\ell, m)\sigma_{33}^{(half-space)}(k, \ell). \qquad (21)$$

The influence coefficients Q_{ij}, (Liu and Wang, 2002), result from integration of Boussinesq formulas over elementary grid cell with respect to directions of $\vec{x}_1$ and $\vec{x}_2$. The product in Eq. (21) is a two-dimensional convolution with respect to directions of $\vec{x}_1$ and $\vec{x}_2$, which can be computed efficiently with DCFFT algorithm.

Finally, the solution for the stress due to arbitrarily shaped eigenstrains in an elastic isotropic half-space results from superposition of solutions (19) and (21).

The two terms in Eq. (19) imply multi-summation over three dimensions, as both source and observation domains are three-dimensional. Computation of these distributions by direct multiplication method (DMM) or even by two-dimensional DCFFT is very time-consuming, therefore a non-conventional approach is required. The first term in Eq. (19) is a three-dimensional convolution, while the second term is a two-dimensional convolution with respect to directions of $\vec{x}_1$ and $\vec{x}_2$ and a one-dimensional correlation with respect to direction of $\vec{x}_3$. Liu and Wang, (Liu & Wang, 2005), suggested that correlation theorem, together with convolution theorem, could be used together in a hybrid convolution-correlation multidimensional algorithm.

In the last decade, spectral methods are intensively used in contact mechanics to rapidly evaluate convolution-type products. These authors, (Jacq et al., 2002), applied a two-dimensional fast Fourier transform algorithm to speed up the computation of convolution products arising in Eq. (19). Their approach reduces the computational requirements from $O(N_1^2 N_2^2 N_3^2)$ in DMM to $O(N_3^2 N_1 N_2 \log N_1 N_2)$.

However, using a two-dimensional algorithm to solve a problem which is essentially three-dimensional is an imperfect solution. Therefore, in this work, a three-dimensional spectral algorithm is implemented, capable of evaluating both convolution and hybrid convolution-correlation type products in $O(N_1 N_2 N_3 \log N_1 N_2 N_3)$ operations. The algorithm, originally advanced in (Spinu & Diaconescu, 2009), is based on the notorious DCFFT technique (Liu et al., 2000).

If the ICs are known in the time/space domain, this algorithm can evaluate the linear convolution by means of a cyclic convolution with no periodicity error. The concepts of "zero-padding" and "wrap-around order", presented in (Liu et al., 2000), can be extended

naturally to the three-dimensional case, and applied to compute the first term in the right side of Eq. (19). However, for the second term, due to positioning of the mirror-image element relative to global coordinate system (linked to half-space boundary), convolution turns to correlation with respect to direction of $\vec{x}_3$. In order to use three-dimensional FFT and convolution theorem to evaluate the convolution-correlation product, the following algorithm is proposed:

1. The influence coefficients $\mathbf{A}$ are computed as a three dimensional array of $N_1 \times N_2 \times 2N_3$ elements, using the formulas derived from Eqs. (16) and (17).
2. The term $\mathbf{A}$ is extended into a $2N_1 \times 2N_2 \times 2N_3$ array by applying zero-padding and wrap-around order with respect to directions of $\vec{x}_1$ and $\vec{x}_2$, as requested by the classic DCFFT algorithm.
3. Plastic strains $\boldsymbol{\varepsilon}^p$ are inputted as a three-dimensional array of $N_1 \times N_2 \times N_3$ elements.
4. The term $\boldsymbol{\varepsilon}^p$ is extended to a $2N_1 \times 2N_2 \times 2N_3$ array by zero-padding in all directions.
5. Elements of $\boldsymbol{\varepsilon}^p$ are rearranged in reversed order with respect to direction of $\vec{x}_3$.
6. The Fourier transforms of $\mathbf{A}$ and $\boldsymbol{\varepsilon}^p$ are computed by means of a three-dimensional FFT algorithm, thus obtaining the complex arrays $\hat{\mathbf{A}}$ and $\hat{\varepsilon}^p$, where ($\hat{g}$) is used to denote the discrete Fourier transform of any time/space array g.
7. The spectral array of residual stresses is computed as element-by-element product between convolution terms: $\hat{\sigma}^{r(space)} = \hat{A} \cdot \hat{\varepsilon}^p$.
8. The time/space array of residual stresses is finally obtained by means of an inverse discrete Fourier transform: $\sigma^{r(space)} = IFFT(\hat{\sigma}^{r(space)})$.
9. The terms in the extended domain are discarded, thus keeping the terms $N_1 \times N_2 \times N_3$ of $\sigma^{r(space)}$ as output.

Domain extension with respect to directions of $\vec{x}_1$ and $\vec{x}_2$ in step 2 is required by the DCFFT technique, and no additional treatment is needed to evaluate the corresponding discrete cyclic convolutions. On the other hand, according to discrete correlation theorem, (Press et al., 1992), a correlation product can be evaluated as a convolution between one member of the correlation and the complex conjugate of the other. Therefore, DCFFT can be applied with respect to direction of $\vec{x}_3$ too, if the second term, namely the plastic strains array, is substituted by its complex conjugates in the frequency domain. The fastest way to achieve this is to rearrange the terms of $\boldsymbol{\varepsilon}^p$, as indicated in step 4. Indeed, when FFT is applied on a series of real terms g, thus obtaining $\hat{g}$, one can obtain its complex conjugate $\hat{g}^*$, simply by reading g in reversed order. This remarkable property allows for combining convolutions and correlations products with respect to different directions in a hybrid algorithm. By applying three-dimensional FFT, the computational effort for solving the inclusion problem in infinite, elastic and isotropic space is reduced considerably, from $O(N_3^2 N_1 N_2 \log N_1 N_2)$ in Jacq's approach to $O(N_1 N_2 N_3 \log N_1 N_2 N_3)$ operations for the newly proposed algorithm.

The following step is to compute the stress state induced in the half-space by spurious normal traction $\sigma_{33}^{(half-space)}$. In existing formulations, (Chiu, 1978; Jacq, 2001), this stresses are expressed explicitly as functions of plastic strains ε_{ij}^p. This rigorous formulation results in increased model complexity. It also has the disadvantage of limiting the application of spectral methods to two-dimensional case. However, if the analysis domain is large enough, one can assume that the normal traction induced on the half-space boundary vanishes outside the computational domain. Therefore, the corresponding elastic state (d) is due to term $\sigma_{33}^{(half-space)}$ alone. With this assumption, computation of elastic state (d) is

reduced to the problem of a stress state induced in an elastic isotropic half-space by an arbitrarily, yet known, pressure (or normal traction). Solution of this problem is readily available, as corresponding Green functions are known from Boussinesq fundamental solutions.

The resulting computational advantage is more effective when using the newly proposed algorithm as part of an elastic-plastic contact code. Indeed, influence coefficients Q_{ij} needed to assess stresses induced by pressure are shared with the elastic contact code. They are computed and stored as a $N_1 \times N_2 \times N_3$ array. In Jacq's formulation, N_3 arrays, each having $N_1 \times N_2 \times N_3$ terms, are needed, because influence coefficients needed to impose free surface relief depend explicitly on both source and computation point depths. This double dependence also limit the use of spectral methods to two dimensions, thus being of order $O(N_3^2 N_1 N_2 \log N_1 N_2)$, corresponding to N_3^2 two-dimensional DCFFTs in layers of constant depth.

In the simplified formulation advanced in this paper, as source domain (namely pressure domain) is only two-dimensional, as opposed to plastic zone, which is three-dimensional, the computational order is decreased to $O(N_1 N_2 N_3 \log N_1 N_2)$ operations, corresponding to N_3 two-dimensional DCFFTs in layers of constant depth.

The method for imposing the pressure-free condition assumes that spurious normal tractions on the half-space boundary vanish outside computational domain. This assumption requires a larger computational domain in order to minimize truncation errors. When simulating concentrated elastic-plastic contacts, plastic region is usually located under the central region of the contact area, occupying a hemispherical domain. Therefore, the newly proposed method is well adapted to this kind of problems.

As inclusion problem has to be solved repeatedly in an elastic-plastic contact simulation, the overall computational advantage is remarkable, allowing for finer grids or smaller loading steps to reduce discretization error.

4.3 Plastic strain increment assessment

According to general theory of plasticity, plastic flow occurrence can be described mathematically with the aid of a yield function, assessing the yield locus in the multidimensional space of stress tensor components. If von Mises criterion is used to assess stress intensity, this function can be expressed as:

$$f(e^p) = \sigma_{VM} - \sigma_Y(e^p) ,$$ (22)

where e^p denotes the effective accumulated plastic strain, $e^p = \sqrt{2\varepsilon_{ij}^p \varepsilon_{ij}^p / 3}$, and $\sigma_Y(e^p)$ is the yield strength function. The latter satisfy the relation for the initial yield strength σ_{Y0}:

$$\sigma_Y(0) = \sigma_{Y0} .$$ (23)

For elastic-perfectly plastic materials, relation (23) is verified for any value of e^p. However, for metallic materials, more complex models of elastic-plastic behavior are employed, as the isotropic, or the kinematic hardening laws. The isotropic hardening law of Swift,

$$\sigma_Y(e^p) = B(C + e^p)^n ,$$ (24)

with B, C and n material constants, is used in the current formulation, as it is verified for many metallic materials, (El Ghazal, 1999) and, from a numerical point of view, it has the advantage of being continuously derivable.

The following conditions must be met all the time:

$$f \leq 0; \ de^p \geq 0; \ f \cdot de^p = 0 , \tag{25}$$

with $f = 0$ and $de^p > 0$ corresponding to plastic flow.

According to flow rule, plastic strain increment can be expressed as:

$$d\varepsilon_{ij}^p = de^p \frac{\delta f}{\delta \sigma_{ij}} = de^p \frac{3S_{ij}}{2\sigma_{VM}} , \tag{26}$$

where S_{ij} denotes the deviatoric stress tensor.

The algorithm used to derive the plastic strain increment was advanced by Fotiu and Nemat-Nasser, who developed a universal algorithm for integration of elastoplasticity constitutive equations. As stated in (Fotiu & Nemat-Nasser, 1996), the algorithm is unconditionally stable and accurate even for large load increments, as it takes into account the entire non-linear structure of elastoplasticity constitutive equations. These are solved iteratively, via Newton-Raphson numerical method, at the end of each loading step. The yield function f is linearized at the beginning of the load increment, by employing an elastic predictor. This places the predictor (trial) state far outside the yield surface $f = 0$, since elastic-plastic modulus is small compared to the elastic one. The return path to the yield surface is generated by the plastic corrector, via Newton-Raphson iteration. This approach, also referred to as elastic predictor - plastic corrector, is efficient when most of the total strain is elastic. In the fully plastic regime, which occurs usually after the elastic-plastic one, the plastic strain is predominant, thus the return path may require numerous iterations. Thus, linearization at the beginning of the loading step is performed by a plastic predictor, and return path is generated with an elastic corrector.

A yield occurs when von Misses stress exceeds current yield stress, namely when $f > 0$. The elastic domain expands and/or translates to include the new state, namely to verify condition $f = 0$. The actual increment of effective accumulated plastic strain should satisfy, in the plastic zone, equation of the new yield surface:

$$f(e^p + \delta e^p) = 0 . \tag{27}$$

Here, δe^p denotes the finite increment of effective plastic strain, as defined in (Jacq, 2001). Relation (27) can be considered as an equation in δe^p, which is solved numerically by Newton-Raphson iteration. To this end, yield surface relation is linearized along plastic corrector direction:

$$f(e^p + \delta e^p) = f(e^p) + \delta e^p \frac{\partial f(e^p)}{\partial e^p} = 0 , \tag{28}$$

yielding the plastic corrector:

$$\delta e^p = -\frac{f(e^p)}{\dfrac{\partial f(e^p)}{\partial e^p}} = \frac{f(e^p)}{\dfrac{\partial \sigma_Y(e^p)}{\partial e^p} - \dfrac{\partial \sigma_{VM}}{\partial e^p}} \ . \tag{29}$$

For isotropic hardening, the derivate of equivalent von Mises stress with respect to effective accumulated plastic strain was derived by Nélias, Boucly and Brunet, (Nélias et al., 2006), from the general equations presented in (Fotiu & Nemat-Nasser, 1996) for rate-dependent elastoplasticity:

$$\frac{\partial \sigma_{VM}}{\partial e^p} = -3G \ , \tag{30}$$

where G is the shear modulus, or the μ Lamé's constant.

With these results, the following return-mapping algorithm with elastic predictor - plastic corrector can be formulated:

1. Acquire the state at the beginning of the loading step and impose the elastic predictor. For elastic-plastic contact problems, this is equivalent to solving an elastic loop without imposing any residual displacement increment. Corresponding parameters are identified by an "a" superscript, as opposed to a "b" superscript, used to denote the state at the end of the loading increment: $e^{p(a)}$, $\sigma_Y^{(a)} = \sigma_Y(e^{p(a)})$, $\sigma_{ij}^{(a)} = \sigma_{ij}^{pr(a)} + \sigma_{ij}^{r(a)}$, $\sigma_{VM}^{(a)}$, $f^{(a)} = \sigma_{VM}^{(a)} - \sigma_Y^{(a)}$. These variables also represent the input for the Newton-Raphson iteration. Thus, by using superscripts to denote the Newton-Raphson iteration number, $e^{p(1)} = e^{p(a)}$, $\sigma_Y^{(1)} = \sigma_Y^{(a)}$, $\sigma_{ij}^{(1)} = \sigma_{ij}^{(a)}$, $\sigma_{VM}^{(1)} = \sigma_{VM}^{(a)}$, $f^{(1)} = f^{(a)}$.

2. Start the Newton-Raphson iteration. Compute the plastic corrector according to relations (29) and (30):

$$\delta e^{p(i)} = f^{(i)} \left/ \left(\frac{\partial k(e^{p(i)})}{\partial e^{p(i)}} + 3G \right) \right. . \tag{31}$$

3. Use the plastic corrector to adjust model parameters:

$$\sigma_{VM}^{(i+1)} = \sigma_{VM}^{(i)} - 3G \delta e^{p(i)} ; \quad e^{p(i+1)} = e^{p(i)} + \delta e^{p(i)} ; \quad \sigma_Y^{(i+1)} = \sigma_Y(e^{p(i+1)}) ; \quad S_{ij}^{(i+1)} = \frac{\sigma_{VM}^{(i+1)}}{\sigma_{VM}^{(1)}} S_{ij}^{(1)} \ . \tag{32}$$

4. Verify if Eq. (27) is verified to the imposed tolerance eps. If condition

$$\left| f^{(i+1)} \right| = \left| \sigma_{VM}^{(i+1)} - \sigma_Y^{(i+1)} \right| > eps \tag{33}$$

is satisfied, go to step 2. If else, convergence is reached, and the state at the end of the loading step is described by the newly computed parameters: $e^{p(b)} = e^{p(i+1)}$, $\sigma_{VM}^{(b)} = \sigma_{VM}^{(i+1)}$, $S_{ij}^{(b)} = S_{ij}^{(i+1)}$.

5. Compute the plastic strain increment, according to Eq. (26):

$$\delta \varepsilon_{ij}^p = \left(e^{p(b)} - e^{p(a)} \right) \frac{3 S_{ij}^{(b)}}{2 \sigma_{VM}^{(b)}} \ . \tag{34}$$

This increment is used to update the plastic zone. The residual parts of displacement and of stress can then be computed, and superimposed to their elastic counterparts.

5. Numerical solution of the elastic-plastic contact problem

Elastic-plastic normal contact problem is solved iteratively based on the relation between pressure distribution and plastic strain, until the latter converges. Plastic strain modifies contact pressure by superposing induced residual surface displacement into the interference equation. Contact pressure, in its turn, contributes to the subsurface stress state, responsible for plastic strain evolution.

Finally, the algorithm proposed for simulation of elastic-plastic contact with isotropic hardening is based on three levels of iteration:

1. The innermost level, corresponding to the residual part, assesses plastic strain increment, based on an algorithm described in the previous section, and the contribution of plastic zone to stress state and surface displacement.
2. The intermediate level adjusts contact pressure and residual displacement in an iterative approach specific to elastic contact problems with arbitrarily shaped contact geometry.
3. The outermost level is related to the fact that, unlike elastic solids, in which the state of strain depends on the achieved state of stress only, deformation in a plastic body depends on the complete history of loading. Plasticity is history dependent, namely current state depends upon all pre-existing states. In this level, the load is applied in finite increments, starting from an intensity corresponding to elastic domain, until the imposed value is reached.

The algorithm for solving one loading step in the elastic-plastic normal contact problem is summarized in Fig. 2.
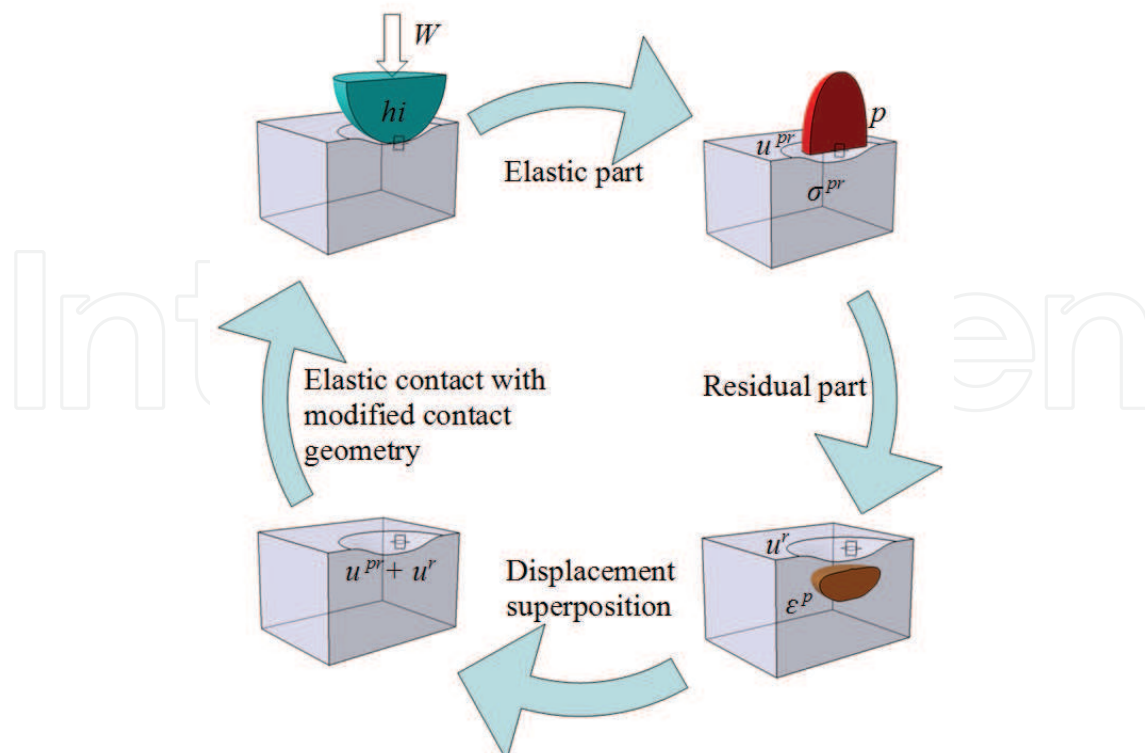
Fig. 2. Elastic - plastic algorithm

Firstly, the elastic problem with modified contact geometry hi is solved, yielding contact area and pressure distribution p. The latter is used to assess elastic displacement field u^{pr} and stress field σ^{pr}. These terms represent the "elastic" part of displacement and of stress, namely that part that is recovered once loading is removed (after contact opening). The stresses induced by pressure are used, together with hardening state parameters, in the residual subproblem, to assess plastic strain increment and to update the achieved plastic zone ε^p. Residual parts of displacement, u^r, and of stresses, σ^r, can then be computed. As opposed to their elastic counterparts, the terms u^r and σ^r express a potential state, that would remain after contact unloading, if no plastic flow would occur during load relief. The total displacement can then be computed, $u^{pr} + u^r$, thus imposing a new interference equation in the elastic subproblem. These sequences are looped until convergence is reached.

The new algorithm for computation of plastic strain increment improves dramatically the speed of convergence for the residual subproblem. The formulation advanced by Jacq, (Jacq, 2001), based on the Prandtl-Reuss algorithm, implies iteration of a tensorial parameter, namely the plastic strain increment, as opposed to the new algorithm, which iterates a scalar, namely the increment of effective accumulated plastic strain. Convergence of the Newton-Raphson scheme is reached after few iterations. As stated in (Fotiu & Nemat-Nasser, 1996), the method is accurate even for large loading increments.

Moreover, Jacq's algorithm is based on the reciprocal adjustment between plastic strain and residual stress increments. Consequently, at every iteration of the residual loop (the innermost level of iteration), it is necessary to express the residual stress increment. Its assessment implies superposition, with both source (integration) and observation domains three-dimensional. Although three-dimensional spectral methods were implemented to speed up the computation, the CPU time and memory requirements remain prohibitively high.

In the new algorithm, residual stresses due to plastic zone needs to be evaluated at every iteration of the elastic loop (the intermediate level of iteration), after plastic zone update with the new plastic strain increment. In other words, residual stress assessment is moved to an upper iterative level, resulting in increased computational efficiency. Consequently, with the same computational effort, a finer grid can be imposed in the numerical simulations, thus reducing the discretization error.

6. Numerical simulations and program validation

In this section, numerical predictions of the newly proposed algorithm are compared with already published results, validating the computer code. The materials of the contacting bodies are assumed to be either rigid (R), or elastic (E), or elastic-plastic (EP), having a behavior described by a power hardening law (Swift), or elastic-perfectly-plastic (EPP). Four types of contacts are considered: R-EP, E-EP, EP-EP with symmetry about the common plane of contact and R-EPP.

Development of plastic region and of residual stresses with application of new loading increments is assessed, and contribution of residual state, which superimpose elastic state induced by contact pressure, is suggested.

Algorithm refinements allow for a fine grid, of $120 \times 120 \times 80$ elementary cells, to be imposed in the computational domain.

6.1 R-EP contact

The contact between a rigid sphere of radius $R = 105 \cdot 10^{-6} m$ and an elastic-plastic half-space is simulated, allowing for comparison with results published by Boucly, Nélias, and Green, (Boucly et al., 2007). Elastic half-space parameters are: Young modulus, $E_2 = 210 GPa$, Poisson's ratio, $v_2 = 0.3$. The hardening law of the elastic-plastic material is chosen as a power law (Swift), according to (El Ghazal, 1999), Eq. (24), with e^p the effective accumulated plastic strain, expressed in microdeformations, and the following parameters: $B = 1,280 MPa$, $C = 30$, $n = 0.085$.

The contact is loaded incrementally up to a maximum value of $W = 0.65 N$, for which the purely elastic model (Hertz) predicts a contact radius $a_H = 6.053 \mu m$ and a hertzian pressure $p_H = 8,470 \, MPa$.

Dimensionless coordinates are defined as ratios to a_H, $\bar{x}_i = x_i / a_H$, and dimensionless pressure or stresses as ratios to p_H. The computational domain is a rectangular cuboid of sides $L_1 = L_2 = 3a_H$, $L_3 = 1.6a_H$, which is dicretized with the following parameters: $N_1 = N_2 = 120$, $N_3 = 80$ elementary grid cells. Due to the fact that problem is axisymmetric, three dimensional distributions are depicted in the plane $x_2 = 0$ only.

Pressure profiles predicted by the numerical program for six loading levels corresponding to elastic-plastic domain are depicted in Fig. 3. Hertz pressure corresponding to maximum load is also plotted for reference.
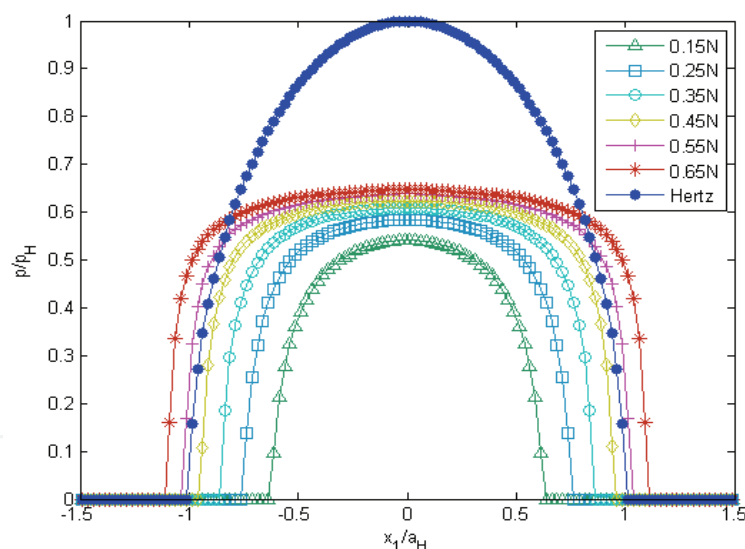
Fig. 3. Pressure profiles in the plane $x_2 = 0$, various loading levels

Elastic-plastic pressure distributions appear flattened compared to the purely elastic case. At the end of the loading loop, a central plateau of uniform pressure can be observed in the vicinity of $6.5p_H$. This limitation of contact pressure results in an increased elastic-plastic contact radius, compared to its elastic counterpart, a_H.

The same distributions were obtained by Jacq et al., (Jacq et al., 2002), by Boucly, Nélias, and Green, (Boucly et al., 2007), using load driven (ld) or displacement driven (dd) formulations, and also by Benchea and Cretu, (Benchea & Cretu, 2008), using finite element analysis (FEA).

Initiation of plastic flow occurs on the contact axis, where von Mises equivalent stress firstly exceeds initial yield strength. With application of new loading increments, plastic zone

expands to a hemispherical domain, Fig. 4, while material hardening state is modified according to Eq. (24).

Toward the end of the loading cycle, the plastic core approach peripherally the free surface, enveloping an elastic core. Evolution of maximum effective accumulated plastic strain with loading level is presented in Fig. 5.

The model assumes elastic and plastic strains are of the same order of magnitude, corresponding to elastic-plastic range. As plastic strains are small, usually less than 2%, they can be considered small strains and can be superimposed to their elastic counterparts. This approach cannot be applied to larger plastic strains, corresponding to fully plastic range, solution of this scenario requiring FEA.
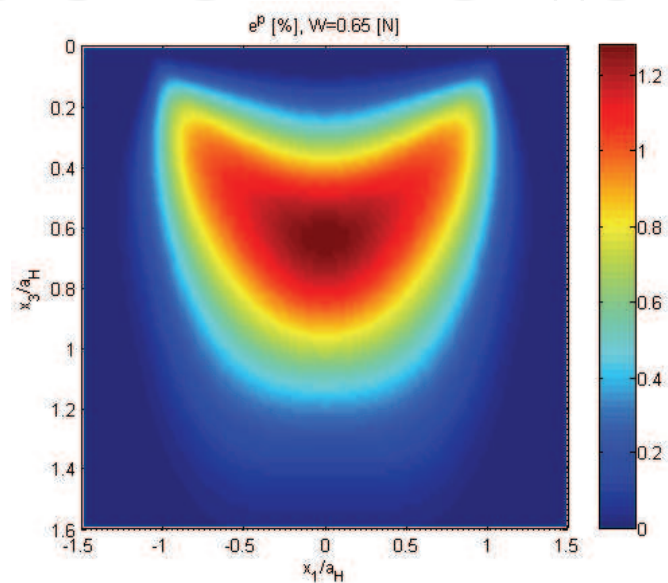
Fig. 4. Effective accumulated plastic strain at $W = 0.65N$
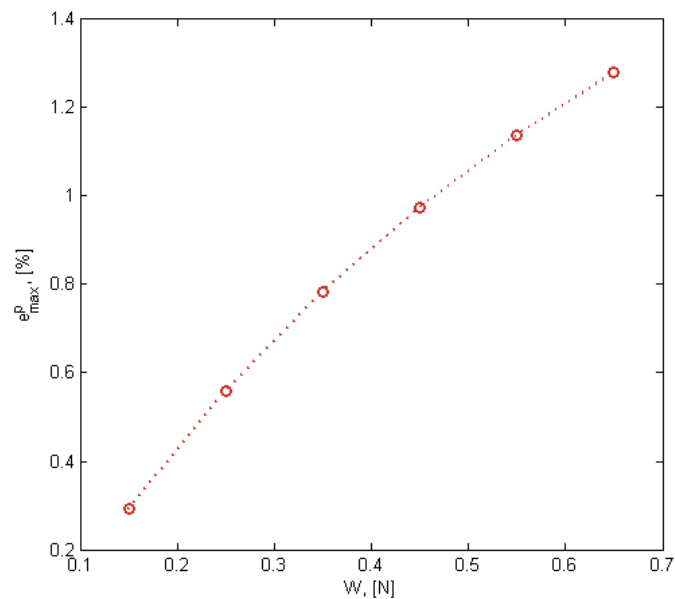
Fig. 5. Maximum effective accumulated plastic strain versus loading level

Plastic strains induce residual stresses, namely elastic stresses that would persist after elastic unloading. These stresses superimpose the ones induced by contact pressure. The resulting state generates further plastic strain if stress intensity exceeds yield strength. Consequently, an accurate estimation of stress field in the elastic-plastic body is essential to plastic strain increment prediction.

Figures 6 and 7 depict distributions of equivalent von Mises contact stress (stress induced by contact pressure) and total stress in the elastic-plastic half-space. Residual stress intensity, Fig. 8, is one order of magnitude smaller than equivalent contact stress. Comparison of distributions depicted in Figs. 6 and 7, using the same scale, suggests that residual stress reduces peaks in contact stress intensity, thus making the resulting field more uniform. This behavior is also suggested by the curves traced in Fig. 9. Maximum intensity of contact stress increase more rapidly than the maximum of the total field, due to contribution of residual stress. Consequently, residual stresses, which represent material response to plastic flow, act to impede further plastic yielding.
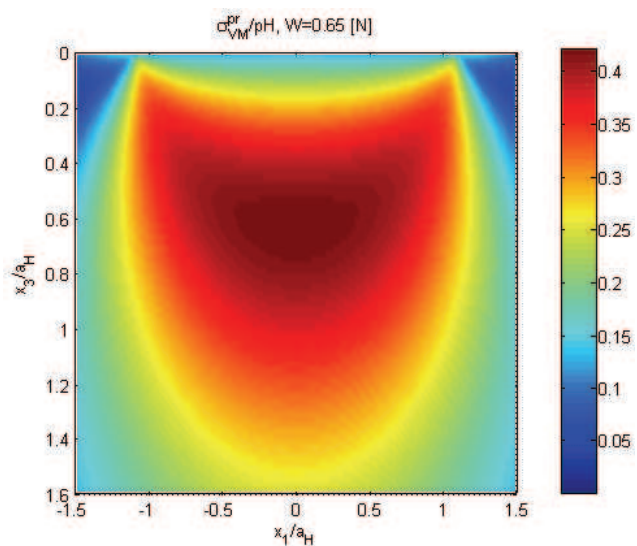
Fig. 6. Von Mises stress induced by contact pressure
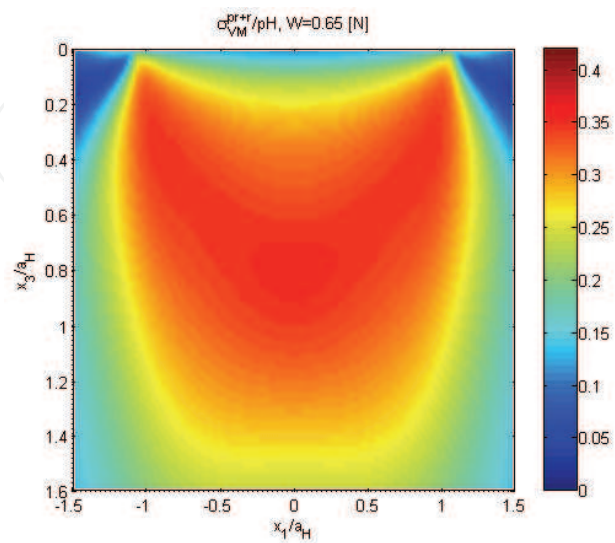
Fig. 7. Maximum intensities of stress fields versus loading level
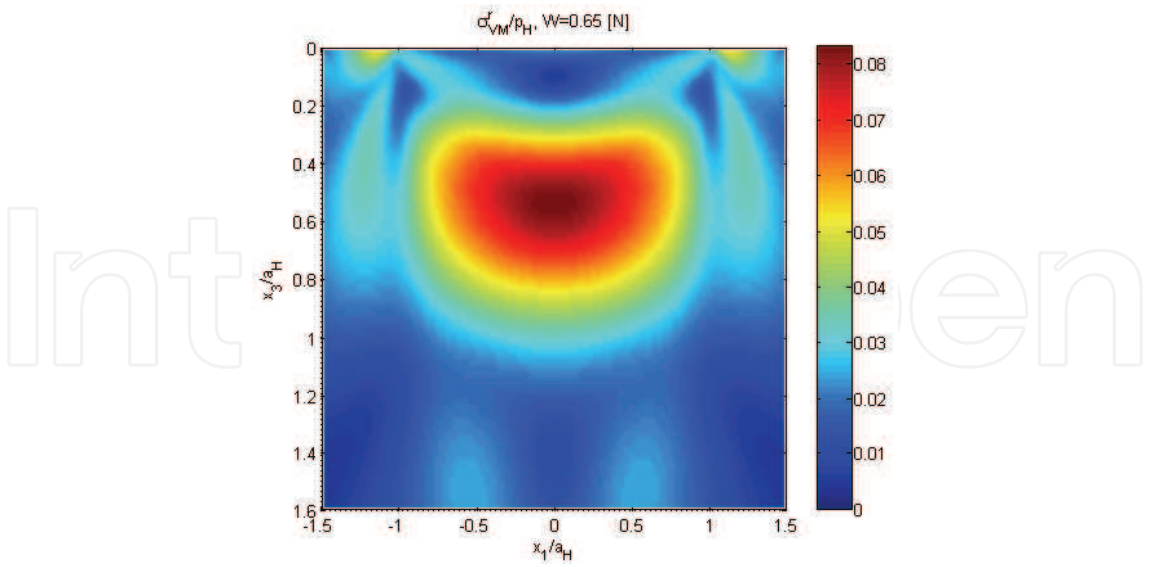
Fig. 8. Von Mises residual stress
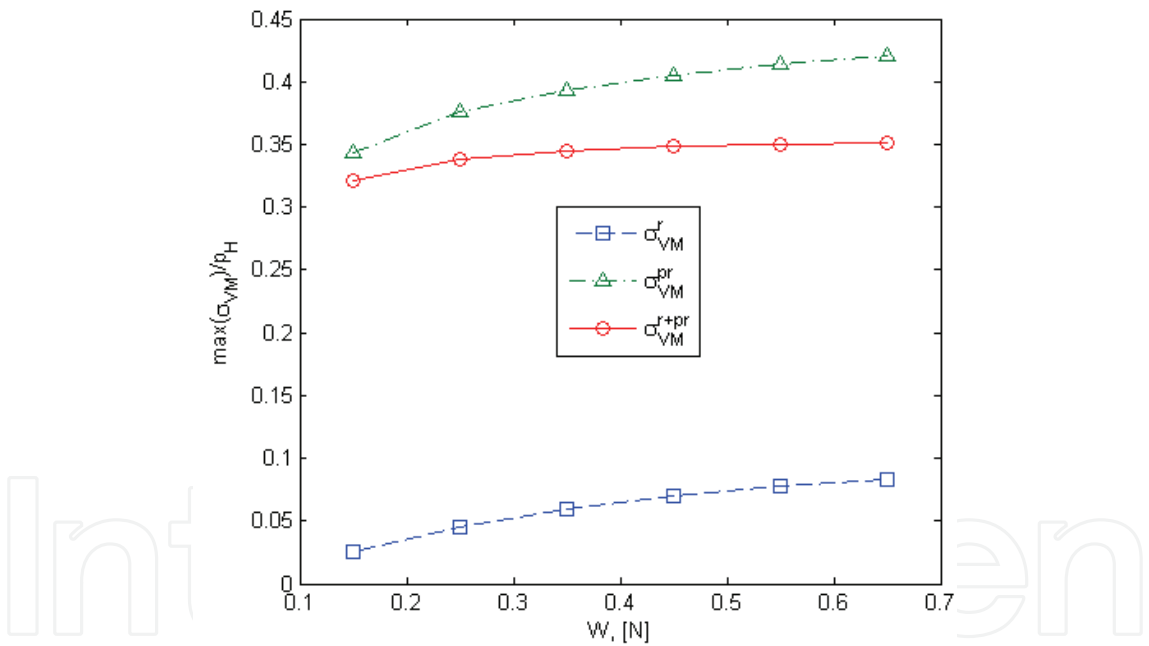
Fig. 9. Total (contact and residual) Von Mises stress in the elastic-plastic body

Profiles of residual prints corresponding to the same six loading levels are depicted in Fig. 10. These profiles show that residual displacement increase contact conformity in investigated non-conforming contact, leading to a more uniform distribution of contact pressure.

The variation of residual print maximum depth with the loading level is presented in Fig. 11. This curve was also obtained experimentally by El Ghazal, (El Ghazal, 1999), numerically by Jacq et al., (Jacq et al., 2002), and using FEA by Benchea and Cretu, (Benchea & Cretu, 2008).
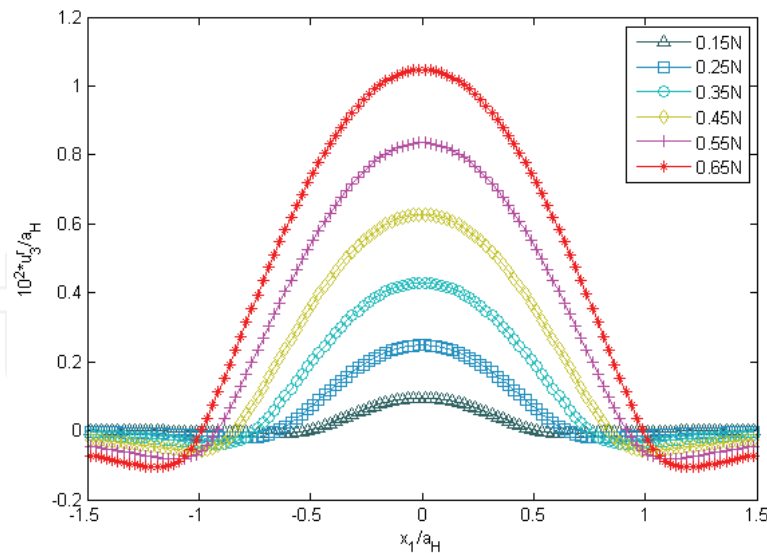
Fig. 10. Residual print profiles in elastic-plastic spherical contact
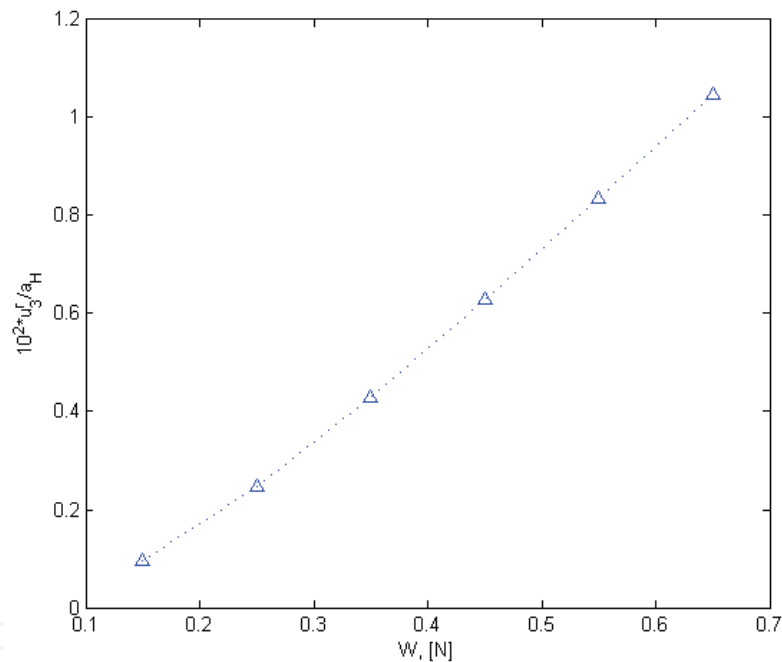
Fig. 11. Residual print depth versus loading level

6.2 E-EP and EP-EP Contact

Normal residual displacement enters interference equation, by superimposing the deflections induced by contact pressure. When only one of the contacting bodies, let it be body (2), is elastic-plastic and the other one, let it be body (1), is elastic, the following interference equation can be written by superimposing the residual part of displacement $u_3^{r(2)}$, related to development of plastic zone in the elastic-plastic body (2), in elastic contact interference relation, Eq. (7):

$$h(i,j) = hi^{(1+2)}(i,j) + u_3^{pr(1+2)}(i,j) + u_3^{r(2)}(i,j) - \omega. \tag{35}$$

On the other hand, when contacting bodies are both elastic-plastic, Eq. (35) encloses residual displacements of both surfaces, namely $u_3^{r(1+2)}(i,j)$. If the hardening behavior or contacting bodies is dissimilar, residual displacement should be computed for every body separately. The model is simplified considerably if the bodies follow the same hardening law and have the same initial contact geometry, because, due to symmetry of the problem about the common plane of contact, $u_3^{r(1)} = u_3^{r(2)}$. Consequently, Eq. (35) becomes:

$$h(i,j) = hi^{(1+2)}(i,j) + u_3^{pr(1+2)}(i,j) + 2u_3^{r(2)}(i,j) - \omega. \tag{36}$$

To validate Eq. (36), the contact between two spheres of radius $R = 0.015m$ is simulated numerically, for two different material behaviors: elastic, and elastic-plastic following Swift's law, with the following parameters: $B = 945MPa$, $C = 20$, $n = 0.121$.

The contact is loaded up to a level of $W = 11,179N$, corresponding to a hertzian pressure $p_H = 8GPa$ and to a Hertz contact radius $a_H = 817\mu m$.

Pressure distributions obtained using Eqs. (35) and (36) respectively, depicted in Fig. 12, agree well with already published results, (Boucly et al., 2007). As expected, in the EP-EP contact, pressure appears more flattened compared to the E-EP case, due to a more pronounced increasing in contact conformity related to doubling of the residual term.
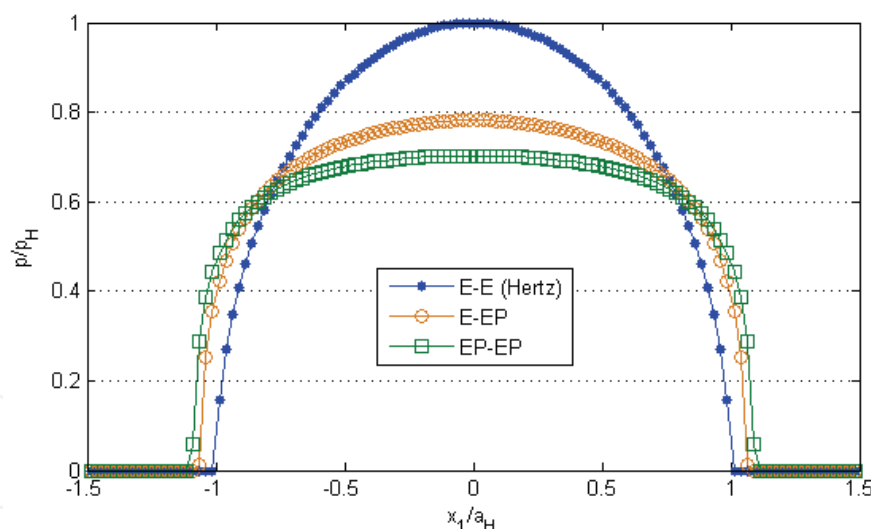
Fig. 12. Pressure profiles for various material behaviors

Variations of maximum effective plastic strain with loading level, in the E-EP and in the EP-EP contact respectively, are depicted in Fig. 13. Intensity of plastic strains in the E-EP contact is up to 40% higher than the one corresponding to the EP-EP scenario.

Variations of maximum pressure with the loading level in the E-E, the E-EP and the EP-EP contact, are depicted in Fig. 14. The curves presented in Figs. 13 and 14 also match well the results of Boucly, Nélias, and Green, (Boucly et al., 2007).
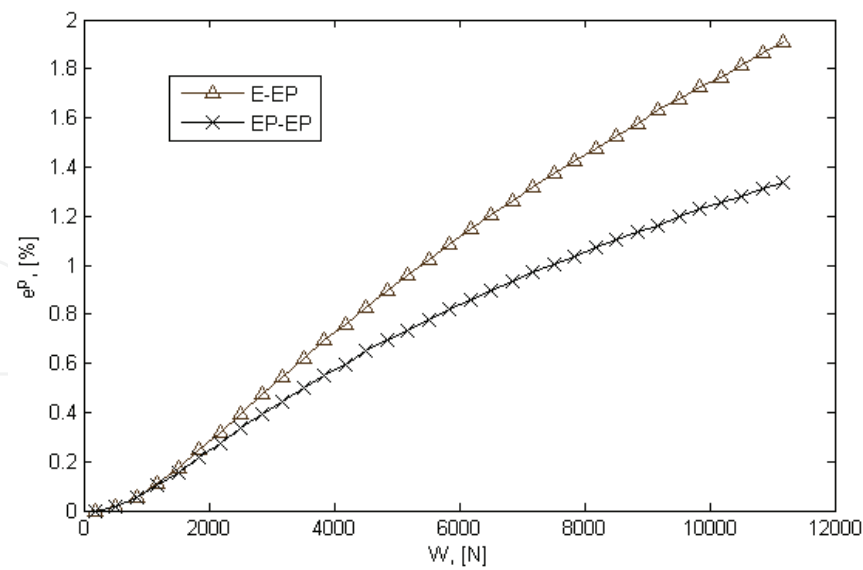
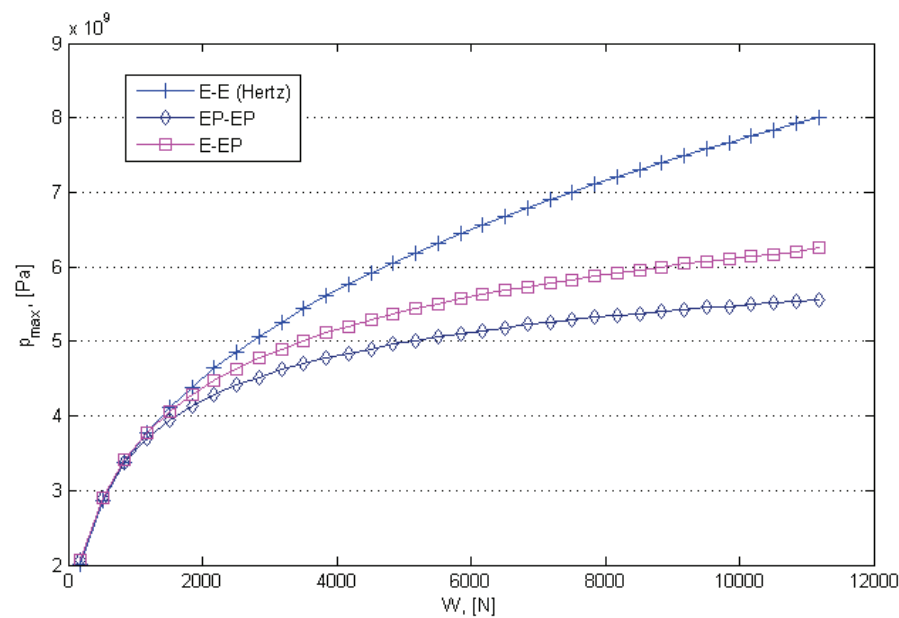Fig. 13. Maximum effective accumulated plastic strain versus loading level

Fig. 14. Maximum pressure versus loading level

6.3 R-EPP contact and experimental validation

As Contact Mechanics uses simplifying assumptions in order to circumvent the mathematical complexity of the arising equations, experimental validation is needed to verify model viability. An extended program of experimental research was conducted in the Contact Mechanics Laboratory of the University of Suceava, aiming to assess residual print parameters in rough elastic-plastic non-conforming contacts. The stand used for the loading experiments was originally designed by Nestor et al., (Nestor et al., 1996). Microtopography of deformed surface was scanned with a laser profilometer UBM14.

Contact between a steel ball, assumed as a rigid indenter, and a lead specimen, simulating the elastic-plastic half-space, was loaded up to an equivalent hertzian pressure

$p_H = 0.94\,GPa$. The contact was also simulated using the numerical formulation. As lead is best described as an EPP material, a linear hardening law with a very small slope was considered in the numerical model. As stated in (Jacq, 2001), the plastic strain increment is undefined when assuming a purely EPP material behavior.

Residual prints at a hertzian pressure of $0.94\,GPa$ is depicted in Fig. 15.
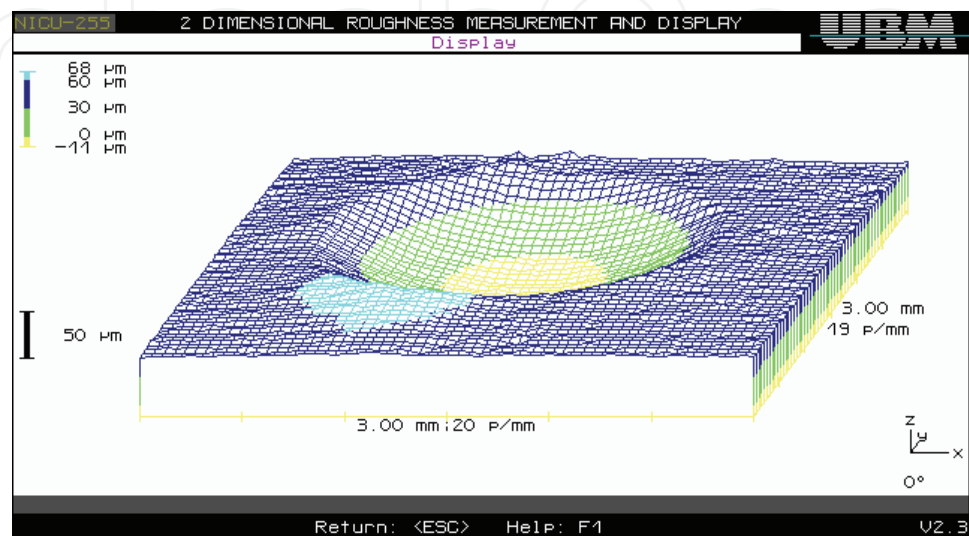
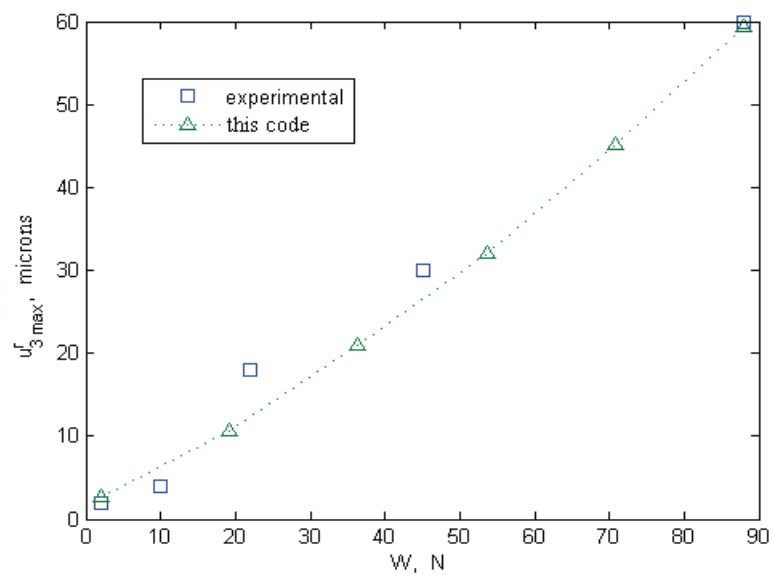Fig. 15. Experimental residual print in R-EPP contact, $p_H = 0.94\,GPa$

Fig. 16. Residual print depth versus loading level

Variation of print depth with loading level is presented in Fig. 16. The agreement between the values predicted numerically and those obtained experimentally is considered satisfactory, giving the complexity of the phenomena involved.

6. Conclusions

A numerical approach for simulating the elastic-plastic contact with isotropic hardening, based on Betti's reciprocal theorem, is overviewed in this paper. Problem decomposition, as originally suggested by Mayeur and later by Jacq, is employed to assess pressure and plastic strain distribution, on three nested iterative levels.

The newly proposed algorithm has two major advantages over other existing methods. Firstly, the plastic strain increment is determined in a fast convergent Newton-Raphson procedure which iterates a scalar, namely the effective accumulated plastic strain. The method, originally suggested by Fotiu and Nemat-Nasser, employs an elastic predictor, which places the trial state outside yield surface, and a plastic corrector, used to derive the return path to the yield locus. The algorithm is fast, stable, and accurate even for large loading increments.

An additional advantage arises from moving residual stress computation, which is very computationally intensive, to an upper iterative level.

Secondly, the use of three-dimensional spectral methods for solving the intrinsically three-dimensional inclusion problem improves dramatically the overall algorithm efficiency. Solution is obtained by problem decomposition, following a method originally suggested by Chiu. Subproblem of stresses due to eigenstrains in infinite space is solved using influence coefficients also derived by Chiu. Traction-free surface condition is imposed with the aid of Boussinesq fundamental solutions, in a simplified formulation, well adapted to elastic-plastic contact modeling.

With the newly advanced three-dimensional convolution and convolution-correlation hybrid algorithm, based on the DCFFT technique, the computational effort is reduced dramatically, allowing for finer grids in problem discretization.

The newly proposed algorithm was used to simulate, with a high resolution of $120 \times 120 \times 80$ elementary cells, the spherical contact between bodies with various behaviors: R-EP, E-EP, EP-EP and R-EPP.

Elastic-plastic pressure appears flattened compared to the elastic case, due to changes in hardening state of the EP material, and in contact conformity due to superposition of residual displacement in interference equation.

Plastic zone, initially occupying a hemispherical region located at hertzian depths, advances toward half-space boundary with increased loading, enveloping an elastic core. This development is consistent with existing models for the elastic-plastic process, marking the passing from elastic-plastic range to fully plastic.

Residual stress intensity is one order of magnitude smaller than equivalent stresses induced by contact pressure. They contribute to total elastic field by decreasing the peaks in contact stress intensity, thus impeding further plastic flow.

A modified interference equation is used for solving the EP-EP contact with similar hardening behavior and symmetry about the common plane of contact.

Furthermore, residual displacement predicted numerically for the R-EPP contact match well print depths obtained experimentally in indentation of a lead specimen, assumed as an EPP half-space, with a steel ball assumed as a rigid indenter.

7. Acknowledgement

8. References

Antaluca, E. (2005). Contribution a l'étude des contacts élasto-plastiques - effet d'un chargement normal et tangentiel. Ph.D. Thesis, INSA Lyon, France.

Benchea, M. & Cretu, S. (2008). An Improved Incremental Model to Analyse Elastic - Plastic Concentrated Contacts – The Finite Element Analysis and Validation. *Acta Tribologica*, Vol. 16, ISSN 1220-8434.

Boucly, V., Nélias, D., & Green, I. (2007). Modeling of the Rolling and Sliding Contact Between Two Asperities. *J. Tribol. (Trans. ASME)*, Vol. 129, pp. 235 - 245.

Boussinesq, J. (1969). *Application des potentiels á l'etude de l'equilibre et du mouvement des solides élastiques*. Reed. A. Blanchard, Paris.

Chen, W. W., Wang, Q. J., Wang, F., Keer, L. M., & Cao, J. (2008). Three-Dimensional Repeated Elasto-Plastic Point Contacts, Rolling, and Sliding. *J. Tribol. (Trans. ASME)*, Vol. 75, pp. 021021-1 - 021021-12.

Chiu, Y. P. (1977). On the Stress Field Due to Initial Strains in a Cuboid Surrounded by an Infinite Elastic Space. *J. Appl. Mech. (Trans. ASME)*, Vol. 44, p. 587-590.

Chiu, Y. P. (1978). On the Stress Field and Surface Deformation in a Half Space with Cuboidal Zone in Which Initial Strains Are Uniform. *J. Appl. Mech. (Trans. ASME)*, Vol. 45, p. 302-306.

El Ghazal, H. (1999). Etude des proprietes microstructurales et mecaniques des aciers 16NiCrMo13 cemente et 32CrMoV13 nitrure - Application a la prevision de leur limite d'endurance en fatigue de roulement. Ph.D. Thesis, INSA Lyon, France.

Fotiu, P. A., & Nemat-Nasser, S. (1996). A Universal Integration Algorithm for Rate-Dependant Elastoplasticity. *Comput. Struct.*, Vol. 59, pp. 1173–1184.

Jacq, C. (2001). Limite d'endurance et durée de vie en fatigue de roulement du 32CrMoV13 nitruré en présence d'indentations. Ph.D. Thesis, INSA Lyon, France.

Jacq, C., Nélias, D., Lormand, G., & Girodin, D. (2002). Development of a Three-Dimensional Semi-Analytical Elastic-Plastic Contact Code. *J. Tribol. (Trans. ASME)*, Vol. 124, pp. 653–667.

Jin, X., Keer, L. M., and Wang, Q. (2008). Note on the FFT Based Computational Code and Its Application. *Proceedings of the STLE/ASME International Joint Tribology Conference IJTC2008*, October 20-22, 2008, Miami, Florida, USA.

Kalker, J. J., van Randen, Y. A.. (1972). A Minimum Principle for Frictionless Elastic Contact with Application to Non-Hertzian Half-Space Contact Problems. *J. Eng. Math.*, Vol. 6(2), pp. 193-206.

Liu, S. B., and Wang, Q. (2002). Studying Contact Stress Fields Caused by Surface Tractions With a Discrete Convolution and Fast Fourier Transform Algorithm. *J. Tribol. (Trans. ASME)*, Vol. 124, pp. 36–45.

Liu, S. B., Wang, Q., & Liu, G. (2000). A Versatile Method of Discrete Convolution and FFT (DC-FFT) for Contact Analyses. *Wear*, Vol. 243 (1–2), pp. 101–111.

Liu, S. Wang, Q. (2005). Elastic Fields due to Eigenstrains in a Half-Space. *J. Appl. Mech. (Trans. ASME)*, Vol. 72, p. 871-878.

Mayeur, C. (1995). Modélisation du contact rugueux élastoplastique. Ph.D. Thesis, INSA Lyon, France.

Mindlin, R. D., & Cheng, D. H. (1950). Thermoelastic Stress in the Semi-Infinite Solid. *J. Appl. Phys.*, Vol. 21, p. 931-933.

Mura, T. (1968). *The Continuum Theory of Dislocation*. Advances in Material Research, Ed. Herman, H., Vol. 3, Interscience Publisher.

Mura, T. (1988). Inclusion Problem. *ASME Applied Mechanics Review*, Vol. 41, pp. 15-20.

Nélias, D., Boucly, V., & Brunet, M. (2006). Elastic-Plastic Contact Between Rough Surfaces: Proposal for a Wear or Running-In Model. *J. Tribol. (Trans. ASME)*, Vol. 128, pp. 236 - 244.

Nestor, T., Prodan, D., Pătraş-Ciceu, S., Alaci, S., & Pintilie, D. (1996). Stand pentru determinarea histerezisului static la solicitarea de contact (in Romanian). *Proceedings of VAREHD 8*, Suceava.

Polonsky, I. A., & Keer, L. M. (1999). A Numerical Method for Solving Rough Contact Problems Based on the Multi-Level Multi-Summation and Conjugate Gradient Techniques. *Wear*, Vol. 231(2), pp. 206–219.

Press, W. H., Teukolsky, S. A., Vetterling, W. T., Flannery, B. P. (1992). *Numerical Recipes in C – The Art of Scientific Computing* – Second Edition. Cambridge University Press.

Shewchuk, J. R. (1994). An Introduction to the Conjugate Gradient Method Without the Agonizing Pain. School of Computer Science, Carnegie Mellon University.

Spinu, S. (2008). A Refined Numerical Method for Elastic Contact Problem with a Tilting Torque on the Contact Area. *Acta Tribologica*, Vol. 16, ISSN 1220-8434.

Spinu, S. (2009). Contributions to the Solution of the Elastic-Plastic Normal Contact Problem (in Romanian), Ph.D. Thesis, University of Suceava, Romania.

Spinu, S., Diaconescu, E. (2008). Numerical Simulation of Elastic Conforming Contacts under Eccentric Loading. *Proceedings of the STLE/ASME International Joint Tribology Conference IJTC2008*, Miami, Florida, USA.

Spinu, S., Diaconescu, E. (2009). A Fast Numerical Method to Predict Elastic Fields Due to Eigenstrains in an Isotropic Half-Space - Part I. Algorithm Overview. *The Annals of University "Dunărea de Jos" of Galati*, Fascicle VIII, 2009 (XV), ISSN 1221-4590, Issue 2, Tribology, pp. 191-196.

Spinu, S., Gradinaru, D. & Marchitan, M. (2007). Improvement of Pressure Distribution in Elastic Non-Hertzian Contacts – Numerical Simulations. *Acta Tribologica*, Vol. 15, ISSN 1220-8434.

Wang, F., & Keer, L. M. (2005). Numerical Simulation for Three Dimensional Elastic-Plastic Contact With Hardening Behavior. *J. Tribol. (Trans. ASME)*, 127, pp. 494–502.

Zhou, K., Chen, W. W., Keer, L. M., & Wang, Q. J. (2009). A Fast Method for Solving Three-Dimensional Arbitrarily Shaped Inclusions in a Half-Space. *Comput. Methods Appl. Mech. Engrg.*, Vol. 198, p. 885-892.
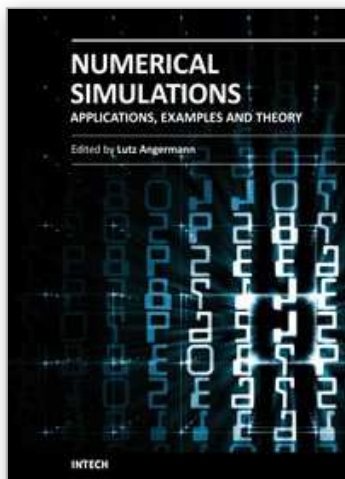
Numerical Simulations - Applications, Examples and Theory

Edited by Prof. Lutz Angermann

This book will interest researchers, scientists, engineers and graduate students in many disciplines, who make use of mathematical modeling and computer simulation. Although it represents only a small sample of the research activity on numerical simulations, the book will certainly serve as a valuable tool for researchers interested in getting involved in this multidisciplinary ï¬eld. It will be useful to encourage further experimental and theoretical researches in the above mentioned areas of numerical simulation.

How to reference

In order to correctly reference this scholarly work, feel free to copy and paste the following:

Sergiu Spinu, Gheorghe Frunza and Emanuel Diaconescu (2011). Numerical Simulation of Elastic-Plastic Non-Conforming Contact, Numerical Simulations - Applications, Examples and Theory, Prof. Lutz Angermann (Ed.), ISBN: 978-953-307-440-5, InTech, Available from: http://www.intechopen.com/books/numerical-simulations-applications-examples-and-theory/numerical-simulation-of-elastic-plastic-non-conforming-contact

INTECH
open science | open minds